

Phase synchronization of chaotic oscillations in terms of periodic orbits

Arkady Pikovsky, Michael Zaks, Michael Rosenblum, Grigory Osipov, and Jürgen Kurths
Department of Physics, University of Potsdam, Am Neuen Palais, PF 601553, D-14415, Potsdam, Germany

(Received 14 May 1997; accepted for publication 10 September 1997)

We consider phase synchronization of chaotic continuous-time oscillator by periodic external force. Phase-locking regions are defined for unstable periodic cycles embedded in chaos, and synchronization is described in terms of these regions. A special flow construction is used to derive a simple discrete-time model of the phenomenon. It allows to describe quantitatively the intermittency at the transition to phase synchronization. © 1997 American Institute of Physics. [S1054-1500(97)02504-4]

When a periodic self-sustained oscillator is governed by a periodic external force, the phenomenon of synchronization can be observed, i.e., the phase of the oscillator is locked to the phase of the driving force. For certain chaotic autonomous dissipative systems the phase can be introduced as well. Such systems can also be synchronized by external periodic force. In this case the phase is locked, while the amplitude remains chaotic. We describe here the phase synchronization of chaotic oscillators through the phase-locking properties of the unstable periodic orbits embedded in a chaotic attractor. For each such orbit the phase-locked region can be constructed, and when these regions overlap, full phase synchronization is observed. Transition to this state is shown to occur via a specific kind of intermittency, arising at the attractor–repeller collision in phase space.

I. INTRODUCTION

Synchronization is a basic nonlinear phenomenon in physics, discovered at the beginning of the modern age of science by Huygens.¹ In the classical sense, synchronization means adjustment or entrainment of frequencies of periodic oscillators due to a weak interaction (cf. Refs. 2–4). This effect is well studied and finds a lot of practical applications in electrical and mechanical engineering.⁵

Extensive investigations of chaotic oscillations have required generalization of the notion of synchronization to this case. In this context, different phenomena have been found which are usually referred to as “synchronization.” Generally, one speaks on synchronization if some nontrivial order is encountered in weakly interacting chaotic systems; e.g. the complete (identical) synchronization is observed if the states of interacting systems coincide while their dynamics remain chaotic; the attractor is then embedded into a symmetrical subspace of the phase space.^{6–8} Another example is the generalized synchronization, where also the dimension of the attractor decreases but the dynamics is restricted to some not necessarily symmetric subspace.^{9–11}

Recently, the effect of *phase synchronization* of chaotic systems has been described theoretically^{12,13} and observed experimentally.¹⁴ It appears in autonomous continuous-time oscillators, where one can introduce the notions of the am-

plitude and the phase even for chaotic motions. Roughly speaking, the amplitude corresponds to a coordinate on a Poincaré surface of section, and the phase increases by 2π during the motion between the cross-sections.¹⁵ The amplitude is chaotic, while the phase is characterized by zero Lyapunov exponent (phase shifts are marginal, like time shifts). The phase synchronization of chaotic system can be defined as the occurrence of a certain relation between the phases of interacting systems (or between the phase of a system and that of an external force), while the amplitudes can remain chaotic and are, in general, uncorrelated. This relation between the phases appears usually as frequency entrainment. It can be easily observed (also experimentally) if one defines the mean frequency of chaotic oscillations as a number of maxima of the process per unit time (more rigorously, one can introduce it as a number of iterations of the Poincaré mapping per unit time). If this frequency coincides or nearly coincides with the frequency of the external force, one can speak of frequency locking. Defined in this way, the phase synchronization appears to be a direct analog of phase locking of periodic oscillations. It describes the onset of long-range correlations in chaotic oscillations (suppression of phase diffusion), and thus also corresponds to the appearance of certain order inside chaos.

Different synchronization transitions can be characterized with the help of the Lyapunov exponents. Because these are the transitions *inside chaos*, the largest Lyapunov exponent remains positive. The transition to complete synchronization happens when a partial (conditional) Lyapunov exponent changes sign. The phase synchronization occurs when the zero Lyapunov exponent becomes negative. It is important, that these transitions occur in a chaotic environment, and therefore are not as “clean” as the order-chaos transitions. In fact, one has to consider these transitions statistically, assuming some characteristic statistical properties of the underlying chaos.

In this paper we exploit the analogy between synchronization of periodic and chaotic oscillations to achieve deeper understanding of structural metamorphoses of strange attractors at the phase synchronization transitions. Our approach is the investigation of phase-locking properties of unstable periodic orbits embedded in strange attractor.¹⁶ For each of this periodic orbits one can define phase-locking regions (Arnold

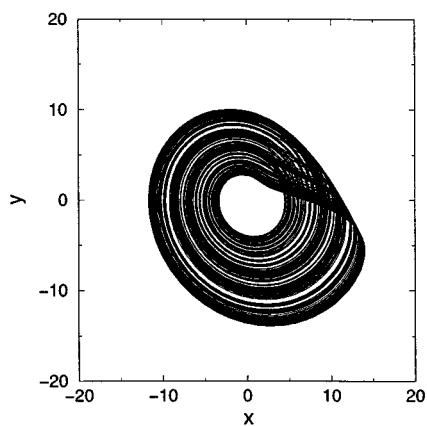


FIG. 1. The phase portrait of the Rössler attractor.

tongues), thus characterizing the phase-locking of the chaotic attractor as a state where all periodic orbits are locked. Correspondingly, the transition to phase synchronization is smeared because generally the Arnold tongues do not coincide. As a result a specific kind of intermittency (which we call “eyelet” since the seldom leakages from the locked state require the very precise hitting of certain small regions in the phase space) is observed at this transition.

The paper is organized as follows. In Section II we introduce the phase synchronization on the example of the externally driven Rössler model. Further, in Section III we describe the special flow construction and reduce the problem to a simple mapping. Study of this mapping as performed in Section IV, allows us to determine the quantitative properties of the synchronization transition. The Rössler model is revisited in Section V where we discuss the correspondences and discrepancies with the derived theoretic implications.

II. PHASE SYNCHRONIZATION IN THE RÖSSLER SYSTEM AND UNSTABLE PERIODIC ORBITS

As an appropriate illustration we take here the Rössler system¹⁷ and act on it with the external force whose amplitude and frequency are given by E and ν , respectively. The resulting equations are:

$$\begin{aligned} \dot{x} &= -z - y + yE \cos \nu t, \\ \dot{y} &= x + ay - xE \sin \nu t, \\ \dot{z} &= xz - cz + b. \end{aligned} \tag{1}$$

Below the parameters $a=0.2$, $c=9$ and $b=1$ are fixed. At these values, the dynamics of the autonomous system (1) is rather simple (Fig. 1) and can be viewed as weakly nonisochronous rotations around the origin. Therefore, one can formally define the phase as

$$\phi = \arctan \frac{y}{x} \tag{2}$$

and calculate the mean observed frequency as

$$\Omega = \langle \dot{\phi} \rangle. \tag{3}$$

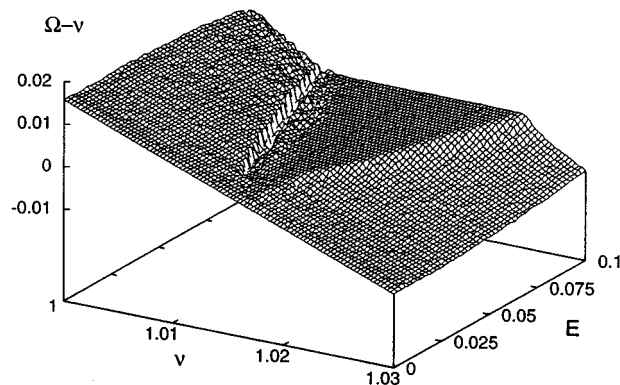


FIG. 2. Phase synchronization of the chaotic Rössler oscillator.

The graph of the observed frequency as a function of the external force amplitude E and the frequency ν allows one to determine the regime of phase synchronization as the state with $\Omega = \nu$. This regime is clearly seen as a large plateau in Fig. 2.

As the unstable periodic orbits (cycles) build a skeleton of the chaotic set, we can attempt to represent the phase synchronization in terms of these cycles. Indeed, periodic external force leads to phase-locking of a cycle, and this is valid both for stable and unstable cycles (only numerics is more cumbersome in the latter case because one has to use special methods to locate an unstable solution). If the frequency of the forcing is close to the frequency of the cycle, the main phase-locking region (the largest Arnold tongue) appears, where two periodic solutions exist having exactly the period of the external force. To classify these solutions it is convenient to look at the Lyapunov exponents. In a dissipative three-dimensional system like (1) an autonomous unstable limit cycle has one positive, one negative, and one zero Lyapunov exponent: $\lambda_+, 0, \lambda_-$. The periodic orbits in the main phase-locking region have the Lyapunov exponents $\lambda_+, \bar{\lambda}_+, \lambda_-$ and $\lambda_+, \bar{\lambda}_-, \lambda_-$ where $\bar{\lambda}_- < 0 < \bar{\lambda}_+$. One can attribute the zero Lyapunov exponent of the autonomous cycle to the phase variable, thus two appearing closed orbits correspond to a stable and unstable position of the phase. At the border of the phase-locking region the orbits with stable and unstable phase disappear through a saddle-node bifurcation.

We want to characterize synchronization of a strange attractor, thus we have to study phase-locking of different periodic orbits embedded in it. First, we need to find these orbits in the autonomous case. To this end a discrete representation of the dynamics is useful, e.g. via the Poincaré map. For the autonomous Rössler system we use the secant surface

$$\dot{y} = 0, \quad x < 0.$$

As the mapping is highly contracting in the z -direction, we get a one-dimensional mapping $x \rightarrow f(x)$ shown in Fig. 3a. This mapping allows us to identify all periodic orbits in the Rössler system and to classify them according to the number of points they produce on the Poincaré map (the number of

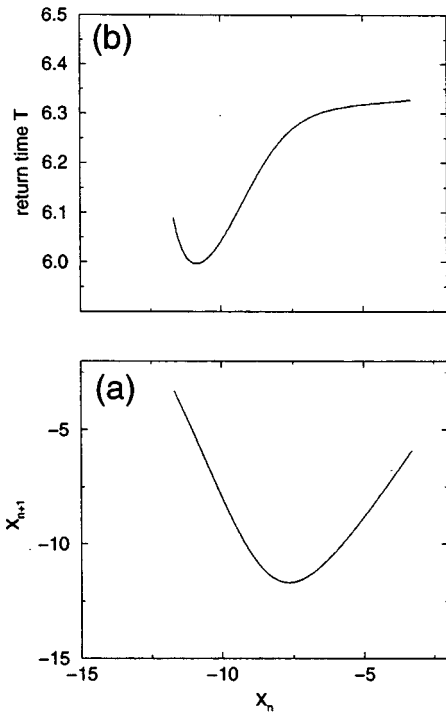


FIG. 3. The Poincaré map (a) and the return times (b) for the autonomous Rössler system.

loops). The latter discrete characteristics we call the orbit's length M . It is clear, that to find the effect of a periodic force, it is not sufficient to know M , but we need to know the real period of the continuous-time orbit T (the mean frequency of the cycle can be then defined as $\omega = 2\pi M/T$). This period cannot be found from the Poincaré map, but requires additional information on the return times between consecutive intersections. We present the return time as a function of coordinate x along the attractor in Fig. 3b. The range in which this differences vary, is not large; nevertheless, as a consequence, the mean frequencies of unstable cycles embedded into the attractor are scattered over the certain (also relatively narrow) interval. (cf. Fig 4 where these frequencies are computed for all the orbits with the length < 15).

In its turn, this implies that the onset of frequency lockings for these orbits should happen at different values of the frequency of external force. It is clear that an adequate description of synchronization must effectively take account for this unequal frequencies.

III. SPECIAL FLOW MODEL

Fortunately, a construction which allows to simplify the problems for the flows with varying return times, is already known. This is the "special flow," or the flow over a mapping.¹⁸ The model is a continuous-time flow in a two-dimensional domain

$$0 \leq x < 1, \quad 0 \leq y < T(x).$$

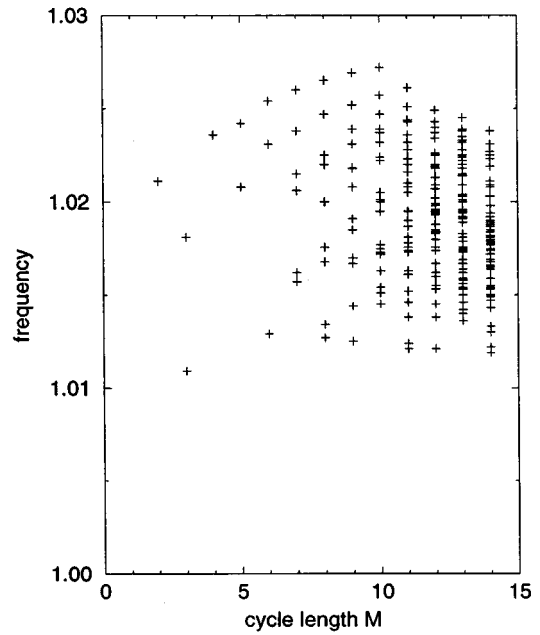


FIG. 4. The mean frequencies for cycles of different lengths in the Rössler model.

The dynamics is defined in the following way: inside the domain one has

$$\dot{y} = 1, \quad \dot{x} = 0, \tag{4}$$

and as the trajectory reaches the boundary point $(x, y = T(x))$, it jumps to the point $(f(x), 0)$ (see Fig. 5). It is easy to see that the mapping $x \rightarrow f(x)$ is the Poincaré map for the flow, and the return time is given by the function $T(x)$. One can take both functions from the simulations for a particular system (in the case of Rössler attractor these should be the dependencies from Fig. 3a and Fig. 3b, respectively) or extract them from the experimental data, thus modeling real dynamics. The advantage of the special flow construction is that here the phase (variable y) and the amplitude (variable x) are separated. If the map $f(x)$ is chaotic and its

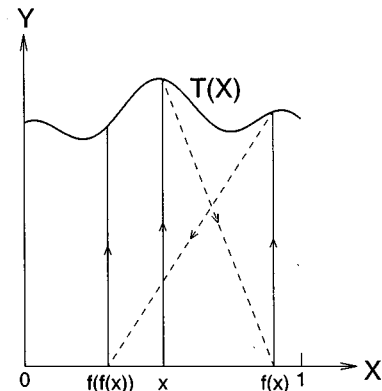


FIG. 5. The special flow construction.

statistical properties are described by the invariant measure $\mu(x)$, then the average frequency of oscillations $\bar{\omega}$ is defined simply as

$$\bar{\omega} = \frac{2\pi}{\langle T(x) \rangle},$$

where the mean period is calculated with respect to μ .

We now generalize the construction by taking into account a periodic external force. First, we introduce the normalized phase according to

$$\phi = y \frac{2\pi}{T(x)}.$$

Next, we assume that the external force having frequency ν and amplitude ε influences only the phase, and not the amplitude x . This approximation is justified at least for small forcing, because the chaotic attractor of the mapping $x \rightarrow f(x)$ is relatively robust with respect to small perturbations, while a marginal position of the phase is sensitive to external influence. Thus, for the phase we write instead of (4) the equation

$$\dot{\phi} = \frac{2\pi}{T(x)} + F(\nu t, \phi), \tag{5}$$

where the function F is 2π -periodic in both arguments. The flow is now defined on the domain $0 \leq x < 1, 0 \leq \phi < 2\pi$ with the jump from the point $(x, 2\pi)$ to the point $(f(x), 0)$.

Let us introduce the phase of the external force according to

$$\psi = \nu t.$$

Then we can rewrite the evolution of ϕ as a two-dimensional flow on a torus

$$\dot{\psi} = \nu, \tag{6}$$

$$\dot{\phi} = \frac{2\pi}{T(x)} + F(\psi, \phi). \tag{7}$$

A natural line of section for this flow is the line $\phi = 0$, and the corresponding Poincaré map can be written as

$$\psi_{n+1} = \psi_n + \nu T(x_n) + \Phi(\psi_n, x_n). \tag{8}$$

Here the nonlinear function Φ is a 2π -periodic function of the first argument. It is determined by the solution of the nonlinear continuous-time equations (6,7) and therefore cannot be generally obtained analytically. [Having the solution $\phi = \phi(t, x_n, \psi_n)$, $\psi = \psi(t, x_n, \psi_n)$ and setting $\phi = 2\pi$ we get the time $t_n(x_n, \psi_n)$ between two intersections. Substitution of this time in the expression for ψ gives the mapping $\psi_{n+1} = \psi_{n+1}(x_n, \psi_n)$.] We can only say that in the case of vanishing forcing $F = 0$ the trajectories on the torus are straight lines, so the function Φ vanishes as well. Thus Φ describes the effect of forcing on the trajectories of the special flow.

We now combine the mapping (8) with the Poincaré map for the amplitude to get finally a discrete-time system that describes the phase synchronization

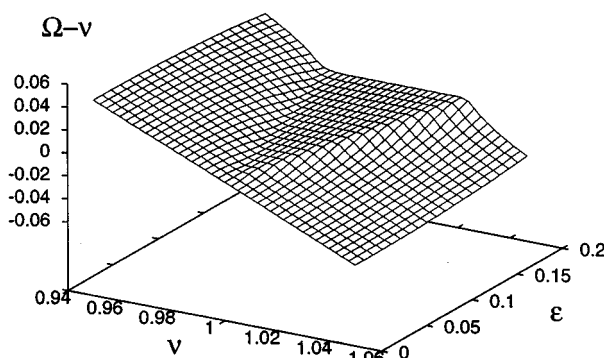


FIG. 6. The synchronization region in system (13) for $\delta = 0.2$.

$$x_{n+1} = f(x_n), \tag{9}$$

$$\psi_{n+1} = \psi_n + \nu T(x_n) + \Phi(\psi_n, x_n). \tag{10}$$

It is worth noting that this is not a stroboscopic map as one could expect for a periodically driven system, but a Poincaré map. Correspondingly, the transformation (10) gives the values of the phase of the external force at the moments when the phase of oscillations is equal to zero. We can define the rotation number for the map (10) as

$$\rho = \lim_{n \rightarrow \infty} \frac{\psi_n - \psi_0}{n}, \tag{11}$$

the frequency of oscillations is then

$$\Omega = \lim_{t \rightarrow \infty} \frac{\phi'(t) - \phi'(0)}{t} = \frac{2\pi}{\rho} \nu \tag{12}$$

(here ϕ' is the phase ϕ lifted onto the whole real line).

Mathematically, the system (9,10) is a skew product: the mapping (9) is not affected by (10). This essentially simplifies the analysis, which we perform in the next section.

IV. MAPPING APPROACH TO PHASE SYNCHRONIZATION

As a concrete example we consider here the following two-dimensional mapping

$$x_{n+1} = f(x_n) = 1 - 2|x_n|, \tag{13a}$$

$$\psi_{n+1} = \psi_n + \nu(T_0 + \delta x_n) + \varepsilon \cos(2\pi\psi_n). \tag{13b}$$

Here ε is the amplitude of the forcing. We assume that the amplitude obeys the tent map, and the phase is governed by the simple chaotically forced circle map. The dependence of the period T on the amplitude x is assumed to be linear. To demonstrate that this map indeed mimics the properties of a real system, we present in Figs. 6 and 7 calculations of the mean rotation number according to (11), which can be compared with the frequency for the Rössler system (Fig. 2). The parameter δ regulates the level of nonisochrony of the oscillations, so that the small values of δ correspond to a phase-coherent attractor.

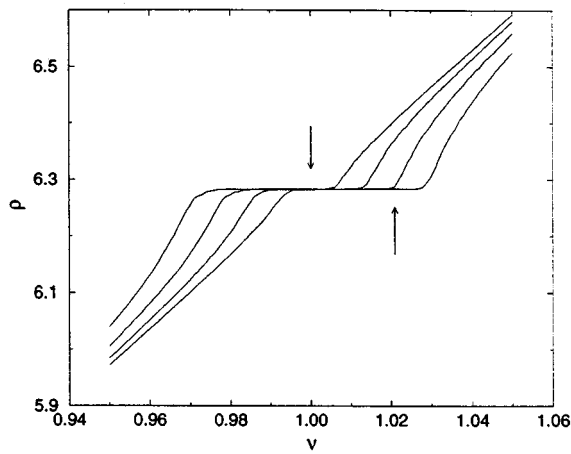


FIG. 7. Dependence of the rotation number ρ on the external parameter ν for the model (13) with $\delta=0.2$ and different forcing amplitudes $\varepsilon=0.2, 0.15, 0.1, 0.05$. The arrows show the attractor–repeller collision points for $\varepsilon=0.2$. Note that the frequency plateau appears to be much larger than the region of full phase synchronization.

We turn now to the representation of a chaotic attractor through unstable periodic orbits embedded in it. Recall that we distinguish between the integer period of the orbit according to the mapping (13a) and the continuous-time period of the flow. The tent map (13a) has periodic orbits of all lengths, and these orbits can be easily found explicitly. If we choose one such orbit, the map (13b) becomes a simple periodically driven circle map, and the classic theory of phase locking (Arnold’s tongues) can be applied.^{19–21} For each periodic orbit in (13a) we can construct the main phase-locked region with the rotation number $\rho=2\pi$. Some of these regions are shown in Fig. 8. The tongues stick into different points on the $\varepsilon=0$ line, because different periodic orbits of the chaotic oscillator have different mean continuous-time periods. In our approach these periods are determined by the average values of the function $T(x)$ on the orbits. For the

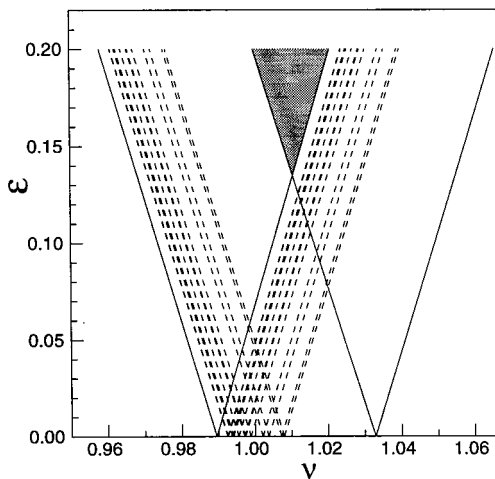


FIG. 8. Phase-locking regions for the fixed points of the tent map (solid lines) and for the periodic orbits with periods 2,3,4,5 (dashed lines) for $\delta=0.1$. The region of full phase synchronization, where all the phase-locking regions overlap, is delineated with grey.

fixed points of the tent map (13a) $x_1 = -1, x_2 = 1/3$ the borders of the phase-locked regions can be easily calculated analytically: $\nu = (2\pi \pm \varepsilon)/(T_0 + \delta x_{1,2})$. For each period- N orbit $x(1), \dots, x(N)$ of the tent map (13a) the dynamics of the phase variable ψ inside the phase-locked region is simple: there exist a corresponding stable $\psi_s(1), \dots, \psi_s(N)$ and an unstable $\psi_u(1), \dots, \psi_u(N)$ orbit. At the border of synchronization these orbits disappear via the saddle-node bifurcation and a state with the rotation number $\rho \neq 2\pi$ appears.

In our case the two fixed points of the tent map play a crucial role, because on these orbits the average value of $T(x)$ reaches the maximum and the minimum, corresponding to the maximal and minimal average continuous-time period of the cycle of the chaotic oscillator. (This is due to the monotonic function $T(x)$ chosen, otherwise the minimum and/or the maximum can be reached by a cycle of high period or even by an aperiodic orbit of the map (13a).) Therefore, the phase-locked regions for all cycles of high periods lie between these “primary” locked regions. A region where all the phase-locked regions overlap is the gray one in Fig. 8. In this region all periodic orbits embedded in the map (13a) are locked, with corresponding stable and unstable orbits of (13) shown in Fig. 9a. These orbits can be considered as skeletons of the attractor and the repeller, respectively, and they are well-separated. All trajectories on the attractor wander in a vicinity of the skeleton, therefore the value of the phase remains bounded, and the rotation number is exactly zero. We call this domain the region of full phase synchronization.

As the parameters of the system are changed in such a way that the boundary of the region of full phase synchronization is approached from inside, the attractor and the repeller come closer to each other. At the transition point of attractor–repeller collision the saddle-node bifurcation for one of the unstable periodic orbits occurs. The situation just beyond the transition is shown in Fig. 9b. Although most cycles remain phase-locked, those few, which have lost phase-locking, allow phase slips to occur (at a slip the phase changes by $\pm 2\pi$). We now develop a statistical theory of these slips (cf. Refs. 22,23).

Consider, for definiteness, the transition at which the phase-locking for the fixed point x_2 is lost. It happens for $\nu_c = (2\pi + \varepsilon)/(T_0 + \delta \cdot x_2)$. Let us first suppose that the value of the variable x in the mapping (13a) is taken exactly at this fixed point, i.e. $x = x_2$ for all times. Then the dynamics of the phase is described by the simple circle map just outside of phase-locking, with characteristic time intervals between phase slips growing as an inverse square root of the distance to the bifurcation point, in the same way as at the type-I intermittency:²⁴

$$\tau_{sl} \approx C_1 (\nu - \nu_c)^{-1/2}. \tag{14}$$

For a chaotic trajectory such a phase slip can also occur, if the trajectory of the tent map (13a) stays for a long time (at least τ_{sl}) in a close vicinity of the fixed point x_2 : $|x - x_2| < C_2$. Suppose that a trajectory of the tent map comes close to the fixed point at time 0: $x(0) \approx x_2$. Because

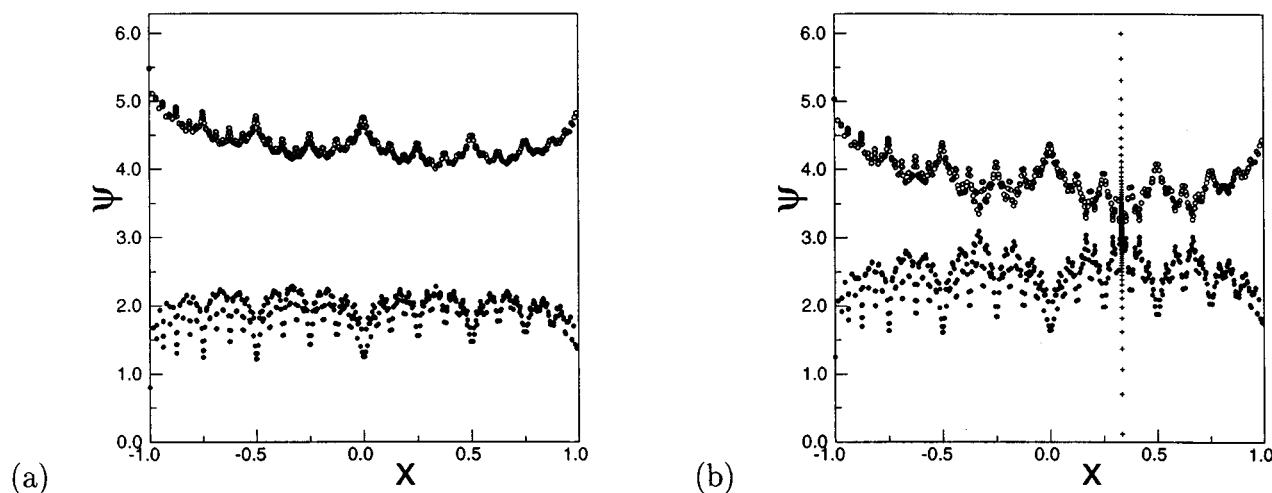


FIG. 9. The stable (filled circles) and unstable (open circles) periodic orbits with periods 1, . . . , 8 forming the skeletons of the attractor and repeller, respectively. (a): inside the full synchronization region $\varepsilon=0.2$, $\delta=0.2$, $\nu=1.01$, the attractor and the repeller are distinct. (b): just after the attractor–repeller collision, at which the stable and unstable fixed points corresponding to $x_2=1/3$ disappear ($\nu=1.0225$). A trajectory of the circle map (13b) with fixed $x=x_2$ is depicted by pluses.

the fixed point of the map (13a) is unstable with the Lyapunov exponent $\lambda(x_2)$ (for the tent map considered, $\lambda = \log 2$), for the evolution of x we can write

$$|x(t) - x_2| \sim |x(0) - x_2| \exp[\lambda(x_2)t].$$

Thus, the condition for the phase slip to occur can be rewritten as

$$|x(0) - x_2| \exp[\lambda(x_2)\tau_{sl}] < C_2$$

which gives the estimate for the slip region in the tent map:

$$|x(0) - x_2| < C_2 \exp[-\lambda(x_2)C_1(\nu - \nu_c)^{-1/2}]. \tag{15}$$

This region is exponentially small, like an “eyelet,” and the phase slips are correspondingly extremely rare. Using the uniform invariant probability density for the tent map we can estimate the probability to visit any interval as proportional to its length. Thus, the probability for a phase slip to occur is proportional to the r.h.s. of (15), and the rotation number is inverse proportional to this probability. As a result, we obtain the following expression for the rotation number at the attractor–repeller collision transition:^{22,23}

$$\log|\rho| \sim -|\nu - \nu_c|^{-1/2}. \tag{16}$$

We check this relation in Fig. 10. It is valid for both transitions where fixed points x_1 and x_2 leave the phase-locked region. From the consideration above it is clear that the time statistics of phase slips corresponds to the statistics of Poincaré recurrence times for a chaotic system (statistics of the returns to the eyelet (15)), and this is known to have the exponential tail.²⁵

The exponentially slow eyelet intermittency is the reason why the phase-locked region for the chaotically driven circle map (Fig. 7) appears to be larger than the region of full phase synchronization, and why the nearly perfect phase synchronization can be observed also for small amplitudes ε , for which there is no full phase synchronization at all. Only

when sufficiently large number of periodic orbits undergoes a saddle-node bifurcation and the probability of phase slip becomes large, one observes a deviation of the mean observed frequency from the frequency of the external force. This also explains the asymmetry of the frequency characteristics Fig. 7: as one can see from Fig. 8, the fixed point x_1 is more isolated in the “skeleton,” compared to the fixed point x_2 ; therefore the probability of phase slips increases more rapidly at the boundary where the fixed point x_2 undergoes the saddle-node bifurcation.

We have considered the simplest possible case when the borders of the region of full phase synchronization are given by the phase-locking regions of the fixed points. This is con-

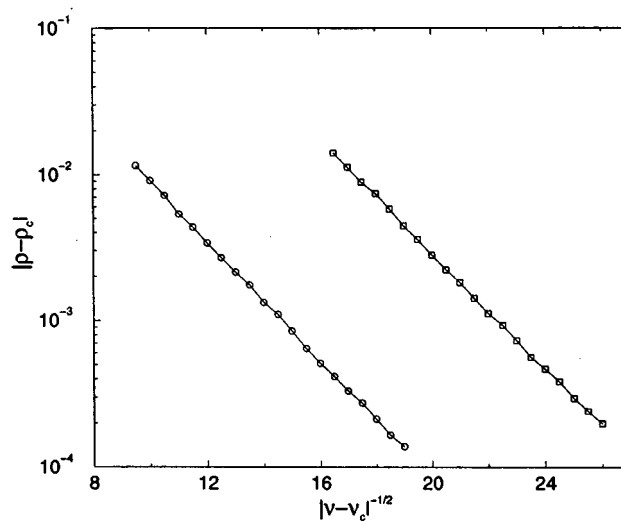


FIG. 10. The rotation number ω at the border of the attractor–repeller transition in the region of eyelet intermittency. The parameters are: $\delta=0.2$, $\varepsilon=0.2$. Squares: the fixed point at x_2 loses stability; circles: the fixed point at x_1 loses stability.

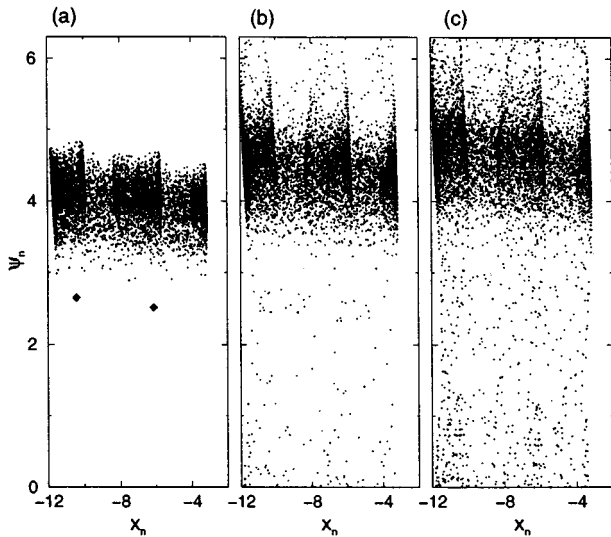


FIG. 11. The Poincaré section in the coordinates x_n, ψ_n . (a): inside the phase-locked region ($E=0.05, \nu=1.018$). The stable (with respect to phase) phase-locked cycle of length 2 is shown with diamonds. (b): near the transition border ($E=0.05, \nu=1.0196$). (c): outside the phase-locked region ($E=0.05, \nu=1.02$).

nected to specific properties of the map $f(x)$ and the function $T(x)$: in the considered above case the maximum and minimum of the averaged period are reached on fixed points of f . The case when these extrema are reached on periodic orbits of $f(x)$ can be considered in a similar way. More complex situations can occur if an extremum is reached on a chaotic everywhere dense trajectory. Then the attractor and the repeller can collide in a dense set of points; similar situation happens in a quasiperiodically forced circle map.^{26,27} This latter case needs special investigation.

V. THE RÖSSLER SYSTEM REVISITED

Now we can compare the data from the forced Rössler system with the conclusions of the preceding section. The similarity between the synchronization plateaus in Fig. 2 and Fig. 6 is not to be overlooked. The Poincaré map induced by the the phase-synchronized attractor on the hyperplane $\dot{y}=0, x<0$ is plotted in Fig. 11a. We present only the coordinate x_n (the coordinate z_n is not important because the attractor is nearly two-dimensional owing to the strong compression along the z -direction). As the second coordinate we use the phase of the external force at the moments t_n of intersections with this plane: $\psi_n = \nu t_n \text{ mod } 2\pi$. This graph is thus analogous to Fig. 9. Outside the transition boundaries, the phase slips are possible and the attractor fills the whole region $0 < \psi_n < 2\pi$ (Fig. 11b,c). These slips contribute to the deviation of the observed frequency Ω from that of the external force ν . Near the transition point $\nu_c(E)$ these deviations are rather rare (Fig. 12), and we observe the scaling of the frequency (Fig. 12):

$$\log|\Omega - \nu| \sim -|\nu - \nu_c|^{-1/2} \tag{17}$$

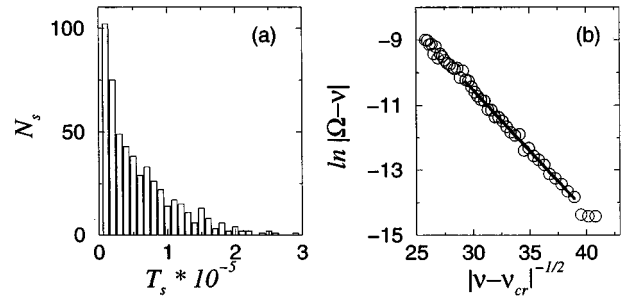


FIG. 12. Statistics of phase slips at the border of full phase locking for the Rössler attractor. (a): A histogram of time intervals between phase slips for $\nu=1.0195, E=0.05$ (b): Frequency difference vs external force frequency near the transition point $\nu_{cr}=1.0185, E=0.05$.

in full accordance with the theoretical prediction (16).

There are, however, peculiarities of the Rössler system that do not fit the picture predicted by the consideration of the special flow model. The location of the locked regions for the particular periodic orbits embedded in the attractor (Fig. 13), reveals the discrepancy with the phase synchronization region calculated for the full system. The phase synchronization can be observed already below the intersection of the outermost tongues, i.e. in the domain where only a part of periodic orbits is synchronized. However, at the largest computationally times we were unable to detect the contribution of phase slips which should be gained in vicinities of unlocked cycles. Thus, it appears that some cycles do not contribute to the phase rotation. To find a reason for this behavior, we have looked at the positions of this cycles in the phase space. It appears that these cycles lie outside of the attractor. E.g., in Fig. 11a it is demonstrated that such a cycle (the cycle of length 2) lies in a completely white area with

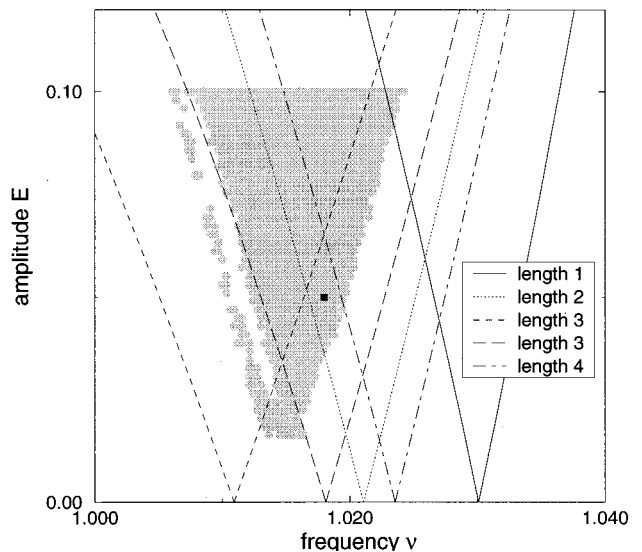


FIG. 13. The phase-locking regions for some cycles in the Rössler model and the region of phase synchronization for the attractor (grey area; this region is extracted from the Fig. 2). The black square marks the parameters used in Fig. 11a; here the cycle of length 2 and one of the cycles of length 3 are locked by the external force.

seemingly no black points around. So although these cycles belong to the attractor, their vicinity is visited extremely rare and possible phase slips are simply not detectable. Why some cycles under influence of forcing “leave” the bulk of the attractor and become “nonobservable,” remains an open question.

VI. DISCUSSION

The transition described can be put in a general framework of bifurcation of strange attractors. At the attractor–repeller collision described the unstable direction is not affected, but in the transversal stable direction the attractor undergoes a “saddle-node” bifurcation. Similar to other bifurcations of strange attractors (e.g., the symmetry-breaking bifurcation discussed in Refs. 28, 29 can be described as a “pitchfork” one) this transition is not abrupt but smeared. The best way to see this is to follow different unstable periodic orbits embedded in a strange attractor: Each of these orbits undergoes the standard saddle-node bifurcation, but at different values of parameters. Remarkably, at both transitions a specific intermittency (modulational one at the symmetry-breaking bifurcation, eyelet intermittency at the attractor–repeller collision) is observed. In terms of phase synchronization the existence of separated attractor and repeller corresponds to full phase-locking, and beyond the collision phase slips are possible (albeit they can be exponentially rare).

It is worth noting that the transition to phase synchronization is also a transition from a nonhyperbolic to a hyperbolic chaos. Indeed, as the unstable periodic orbits inside chaotic attractor become locked, the cycles with different numbers of stable and unstable directions appear. On the other hand, in the hyperbolic attractor all unstable orbits have the same number of unstable directions. Thus, for the attractor to be hyperbolic, it must contain only stable with respect to phase periodic orbits. When this property is not fulfilled, as in Fig. 11b,c, the attracting set is nonhyperbolic.

As a problem for future investigation we would like to mention a characterization of *mutual* phase synchronization in two interacting chaotic systems in terms of periodic orbits. As both systems possess an infinite number of cycles, the problem of their mutual phase-locking appears.

ACKNOWLEDGMENTS

We thank F. Christiansen, R. Friedrich, C. Grebogi, I. Procaccia, J. Sommerer, and J. Yorke for valuable discussions. G.O., M.R., and M.Z. acknowledge support from the Max Planck Society.

- ¹C. Hugenii, *Horologium Oscilatorium* (Parisii, France, 1673).
- ²A. Andronov, A. Vitt, and S. Khaykin, *Theory of Oscillations* (Pergamon, Oxford, 1966).
- ³C. Hayashi, *Nonlinear Oscillations in Physical Systems* (McGraw-Hill, New York, 1964).
- ⁴I. I. Blekhman, *Synchronization of Dynamical Systems* (Nauka, Moscow, 1971) (in Russian).
- ⁵I. I. Blekhman, *Synchronization in Science and Technology* (Nauka, Moscow, 1981) (in Russian); English translation: 1988, ASME Press, New York.
- ⁶H. Fujisaka and T. Yamada, *Prog. Theor. Phys.* **69**, 32 (1983).
- ⁷A. S. Pikovsky, *Z. Phys. B* **55**, 149 (1984).
- ⁸L. M. Pecora and T. L. Carroll, *Phys. Rev. Lett.* **64**, 821 (1990).
- ⁹N. F. Rulkov, M. M. Sushchik, L. S. Tsimring, and H. D. I. Abarbanel, *Phys. Rev. E* **51**, 980 (1995).
- ¹⁰H. D. I. Abarbanel, N. F. Rulkov, and M. M. Sushchik, *Phys. Rev. E* **53**, 4528 (1996).
- ¹¹L. Kocarev and U. Parlitz, *Phys. Rev. Lett.* **76**, 1816 (1996).
- ¹²M. Rosenblum, A. Pikovsky, and J. Kurths, *Phys. Rev. Lett.* **76**, 1804 (1996).
- ¹³A. Pikovsky, M. Rosenblum, and J. Kurths, *Europhys. Lett.* **34**, 165 (1996).
- ¹⁴U. Parlitz, L. Junge, W. Lauterborn, and L. Kocarev, *Phys. Rev. E* **54**, 2115 (1996).
- ¹⁵A. Pikovsky, M. Rosenblum, G. Osipov, and J. Kurths, *Physica D* **104**, 219 (1997).
- ¹⁶A. Pikovsky, G. Osipov, M. Rosenblum, M. Zaks, and J. Kurths, *Phys. Rev. Lett.* **79**, 47 (1997).
- ¹⁷O. E. Rössler, *Phys. Lett. A* **57**, 397 (1976).
- ¹⁸I. P. Cornfeld, S. V. Fomin, and Y. G. Sinai, *Ergodic Theory* (Springer, New York, 1982).
- ¹⁹V. I. Arnold, *Trans. Am. Math. Soc.* **42**, 213 (1965).
- ²⁰O. E. Lanford, in *Recent Developments in Mathematical Physics*, edited by H. Mitter and L. Pittner (Springer, Berlin, 1987), pp. 1–17.
- ²¹E. Ott, *Chaos in Dynamical Systems* (Cambridge University Press, Cambridge, 1992).
- ²²C. Grebogi, E. Ott, and J. A. Yorke, *Phys. Rev. Lett.* **50**, 935 (1983).
- ²³C. Grebogi, E. Ott, and J. A. Yorke, *Ergodic Theory & Dynamical Systems* **5**, 341 (1985).
- ²⁴P. Manneville and Y. Pomeau, *Physica D* **1**, 219 (1980).
- ²⁵T. Tél, in *Directions in Chaos*, edited by H. Bai-Lin (World Scientific, Singapore, 1991), Vol. 3, pp. 149–211.
- ²⁶A. Bondeson, E. Ott, and T. M. Antonsen, *Phys. Rev. Lett.* **55**, 2103 (1985).
- ²⁷U. Feudel, J. Kurths, and A. Pikovsky, *Physica D* **88**, 176 (1995).
- ²⁸A. S. Pikovsky and P. Grassberger, *J. Phys. A* **24**, 4587 (1991).
- ²⁹Y.-C. Lai, C. Grebogi, J. A. Yorke, and S. C. Venkataramani, *Phys. Rev. Lett.* **77**, 55 (1996).